Purely thermal wave based nonchemical photopyroelectric gas sensor: Application to hydrogen

Mahendra Munidasa and Andreas Mandelis
Photothermal and Optoelectronic Diagnostics Laboratory, Department of Mechanical Engineering and Center for Hydrogen and Electrochemical Studies (CHES), University of Toronto, Toronto, Ontario M5S 1A4, Canada

(Received 19 August 1993; accepted for publication 16 March 1994)

A commercially available polyvinylidene fluoride (PVDF) pyroelectric film with an optically generated thermal wave field has been introduced as the active device of a new nonchemical photopyroelectric gas sensor. The purely thermal wave based operating mechanism of this gas sensor is in contrast with a similar, surface chemically active Pd-coated device introduced earlier [A. Mandelis and C. Christofides, J. Appl. Phys. **70**, 4496 (1991)]. The sensitivity to a particular gas at low flow rates (<500 ml min^{-1}) is obtained through thermal boundary condition changes introduced by the gas at the film–gas interface, which depend on the thermophysical properties of the gas. The theoretical basis of this device is described. Photopyroelectric voltage amplitude and phase changes due to ambient hydrogen–air mixtures with respect to pure air, obtained through a lock-in amplifier, are also presented. It is shown that the data are in good agreement with the thermal wave theory. Sensitivity to other common gases used in industry and in environmental studies is also discussed.

I. INTRODUCTION

In recent years, hydrogen has grown to be one of the most useful gases, leading to considerable research efforts towards the development of hydrogen gas sensors. Most of the detection methods are based on electronic devices and use palladium as the active surface. These devices make use of one or more of the many different effects caused by the absorption and desorption of hydrogen in Pd. Most of these sensors are semiconductor-based[1–4] and require fabrication based on sophisticated, multiple-step processing, and they only behave essentially reversibly under specific conditions of pressure, temperature, geometry, etc. During the last few years, much progress has been made in this laboratory, in developing a new photopyroelectric hydrogen gas sensor[5] using Pd-coated pyroelectric thin films, which has distinct advantages over other sensors under STP conditions.[6,7] It is well known that a potential difference is generated in the direction of poling, between the two electroded surfaces which sandwich a pyroelectric layer [in this case polyvinylidene fluoride (PVDF)] when a temperature change is induced within the pyroelectric layer.[8] A hydrogen sensor has been fabricated by sputter coating Pd metal on PVDF, which adsorbs and subsequently absorbs hydrogen gas molecules preferentially in the presence of other ambient gases due to the high solubility of hydrogen in the palladium matrix. The hypothesis was[9] that, upon establishing an ac steady-state temperature (thermal wave) field within the pyroelectric electret by intensity-modulated laser irradiation, followed by absorption and photothermal energy conversion, any changes in the pyroelectric generation mechanisms in the PVDF, due to interactions with the Pd-absorbed hydrogen, would be registered as changes in the observed pyroelectric signal due to a thermodynamically established potential difference between active (Pd) front, and passive (Ni–Al) back electrodes, thus yielding a hydrogen sensor.

In this paper we describe a novel nonchemical evolution of this detector, where any inexpensive metal electrode such as aluminum can be used instead of Pd. This new sensor is based purely on the difference in thermophysical properties between the detected gas and the ambient. The difference in thermal conductivity of gases has been utilized for decades in gas chromatography (GC)[10] in the form of a thermal conductivity detector (TCD). In the TDC, the change in resistivity due to change in temperature of the hot filament is measured using a Wheatstone bridge. A carrier gas (usually helium or hydrogen) with high thermal conductivity is passed through a cell where the filament is placed. When a small amount of a second gas of lower thermal conductivity is introduced into the flow, temperature of the filament increases due to the poor heat lost into the gas. Since this is purely a dc measurement, signal is affected by drift, the temperature fluctuations of the cell, of the environment and of the sensing elements, by turbulence in the gas flow and by mechanical vibrations.[11] Traces of oxygen in the carrier gas should be carefully eliminated in order to avoid rapid oxidation of the filament.[11] Therefore, this device is not suitable for reliable, reversible, long-term continuous gas detection in an open environment. In a typical TCD, with He carrier gas and a filament current of 175 mA, the filament may reach an equilibrium temperature of 100 °C above the surrounding block temperature. This feature may make it unsafe for hydrogen detection, especially above the critical hydrogen–oxygen mixture, where possible ignition and explosion is of great concern for practical applications.

II. DEVICE PHYSICS

The basic cross-sectional geometry of the sensor is shown in Fig. 1. A PVDF film of thickness L with two metal coatings as electrodes on either side is mounted in a housing

 0034-6748/94/65(6)/1978/5/$6.00

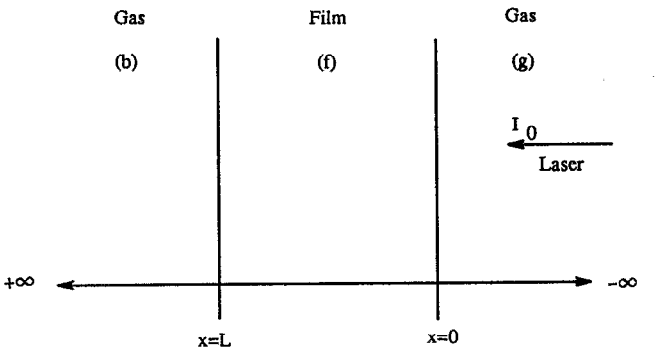

FIG. 1. Basic geometry of the detector. PVDF film (f) of thickness L is surrounded by two semi-infinite regions of gases (g) and (b) on either side.

which allows direct contact with ambient gas(es) on both sides of the film. Although our experiments were performed under a continuous flow of gas (<510 ml min^{-1}), here we assume that the gas is motionless. In fact, experiments have clearly shown that the flow rate of hydrogen does not affect the saturation magnitude of the signal. It only changes the rate at which the signal reaches its maximum. A laser intensity-modulated at angular frequency ω illuminates one side of the film generating a thermal wave profile across the thickness of the film. The laser spot-size on the film is assumed to be wide enough compared to L so that one-dimensional thermal wave propagation is satisfied. This condition is easy to attain using 9–52 μm thick PVDF and an unfocused laser beam.

The pyroelectric voltage which is proportional to the average temperature of the film for a given a gas can be calculated by solving coupled one-dimensional heat diffusion equations subject to a harmonically oscillating thermal flux $F_0(\omega)=\eta I_0[1+\exp(i\omega t)]/2$ at the PVDF-gas interface $x=0$, with appropriate boundary conditions, in each region (g), (f), and (b) (Fig. 1). Here $\eta\simeq 1$ is the optical-to-thermal energy conversion efficiency of the PVDF surface electrode exposed to the laser beam, I_0 is the optical irradiance, and ω is the beam intensity modulation angular frequency. The solution, ac temperature T_j, to the diffusion equation in each medium can be written as

$$T_g(x,\omega)=C_1\exp(\sigma_g x), \quad 0\geqslant x, \tag{1}$$

$$T_f(x,\omega)=C_2\exp(-\sigma_f x)+C_3\exp(\sigma_f x), \quad 0\leqslant x\leqslant L, \tag{2}$$

$$T_b(x,\omega)=C_4\exp[-\sigma_b(x-L)], \quad x\geqslant L, \tag{3}$$

where

$$\sigma_j=(1+i)\sqrt{\frac{\omega}{2\alpha_j}} \tag{4}$$

for the jth medium, and α_j is the thermal diffusivity of that medium. The thickness-averaged temperature of the film is given by

$$\tilde{T}_f(\omega)=\frac{1}{L}\int_0^L T_f(x,\omega)dx$$

$$=\frac{1}{L}\left[C_2\int_0^L \exp(-\sigma_f x)dx+C_3\int_0^L \exp(\sigma_f x)dx\right]. \tag{5}$$

Applying boundary conditions of (a) continuity of the temperature and (b) conservation of the heat flux, at $x=0$ and $x=L$ results in the following equations, which allow us to solve for C_2 and C_3:

$$T_f(0,\omega)=T_g(0,\omega), \tag{6}$$

$$T_f(L,\omega)=T_b(L,\omega), \tag{7}$$

$$-k_f T_f'(x,\omega)|_{x=0}+k_g T_g'(x,\omega)|_{x=0}=\frac{1}{2}\eta I_0, \tag{8}$$

$$k_f T_f'(x,\omega)|_{x=L}=k_b T_b'(x,\omega)|_{x=L}, \tag{9}$$

where k_j are the thermal conductivities and T_j' represents the spatial derivative of temperature. $Q_0\equiv\eta I_0/2$ represents the thermal flux imparted to the PVDF film surface facing the laser source. Solving Eqs. (1)–(4) and (6)–(9) for C_2 and C_3 and substituting in Eq. (5) yields

$$\tilde{T}_f(\omega)=\frac{Q_0}{Lk_f\sigma_f^2}\frac{[1+b_{bf}+(1-b_{bf})\exp(-\sigma_f L)][1-\exp(-\sigma_f L)]}{[(1+b_{gf})(1+b_{bf})-(1-b_{gf})(1-b_{bf})\exp(-2\sigma_f L)]}, \tag{10}$$

where

$$b_{ij}=\frac{k_i\sigma_i}{k_j\sigma_j}=\frac{k_i}{k_j}\sqrt{\frac{\alpha_j}{\alpha_i}}=\frac{\sqrt{\rho_i c_i k_i}}{\sqrt{\rho_j c_j k_j}}, \tag{11}$$

with $\rho_j(c_j)$ being the density (specific heat) of material j. Since both sides of the film are exposed to the same gas, it follows that $b_{gf}=b_{bf}$. The ratio of the complex signals when the detector is placed in two different gases $g1$ and $g2$ is [from Eq. (10)]

$$\frac{T(\omega)_{g1}}{T(\omega)_{g2}}=\frac{(1+b_{g2})[1-\gamma_{g2}\exp(-\sigma_f L)]}{(1+b_{g1})[1-\gamma_{g1}\exp(-\sigma_f L)]}, \tag{12}$$

where

$$\gamma_{ij}\equiv\frac{1-b_{ij}}{1+b_{ij}}. \tag{13}$$

Separating the real and the imaginary parts of Eq. (12), the ratio of the amplitudes with 100% hydrogen, $A_{H2}(\omega)$, and with 100% air, $A_{air}(\omega)$, is given by

$$\frac{A_{H2}(\omega)}{A_{air}(\omega)} = \frac{(1+b_{air})}{(1+b_{H2})} \sqrt{\frac{[1-\gamma_{air}\exp(-a_f L)\cos a_i L]^2+\gamma_{air}^2\exp(-2a_f L)\sin^2 a_f L}{[1-\gamma_{H2}\exp(-a_f L)\cos a_f L]^2+\gamma_{H2}^2\exp(-2a_f L)\sin^2 a_f L}} \tag{14}$$

and the phase difference is given by

$$\theta_{H2}(\omega)-\theta_{air}(\omega)=\tan^{-1}\left[\frac{\gamma_{air}\exp(-a_f L)\sin a_f L}{1-\gamma_{air}\exp(-a_f L)\cos a_f L}\right] - \tan^{-1}\left[\frac{\gamma_{H2}\exp(-a_f L)\sin a_f L}{1-\gamma_{H2}\exp(-a_f L)\cos a_f L}\right], \tag{15}$$

where

$$a_f = \sqrt{\frac{\omega}{2\alpha_f}}. \tag{16}$$

The behavior of the amplitude ratio and the phase difference as a function of the laser modulation frequency is shown in Figs. 2(a) and 2(b) (solid lines), respectively. The following thermophysical parameters have been used in calculating those curves: $k_{air}=26.14\times10^{-3}$ W m^{-1} K^{-1} $\alpha_{air}=22.03\times10^{-6}$ m^2 s^{-1}, $k_{H2}=182\times10^{-3}$ W m^{-1} K^{-1}, $\alpha_{H2}=155.4\times10^{-6}$ m^2 s^{-1} (Ref. 10), $k_f=190\times10^{-3}$ W m^{-1} K^{-1}, $\alpha_f=8\times10^{-8}$ m^2 s^{-1} (Ref. 12). A film of thickness 28 μm has been assumed, reflecting the experimental situation. The signals calculated at 21 Hz, for several gases other than H_2 with respect to air are tabulated in Table I.

III. EXPERIMENT

A schematic diagram of the experimental setup is shown in Fig. 3(a). A commercial PVDF film of thickness 28 μm with Ni/Al electrodes on either side[8] was installed in a commercially available INFICON™ housing with sufficient access to gases from both sides. Light from an intensity-modulated laser diode with variable frequency was guided on to the back of the film using an optical fiber, Fig. 3(b). The sensor was placed inside a chamber which permitted the controlled continuous flow of gas over the sensor. The signal from the film was preamplified and then connected to a lock-in amplifier, which was interfaced to a computer to record both amplitude and phase. Different concentrations of hydrogen in air mixtures can be introduced via a plastic tubing manifold into the chamber by controlling the flow rate of each gas mixture. Photopyroelectric amplitude and phase signals at 11 Hz for several cycles of 100% hydrogen and 100% air are shown in Figs. 4(a) and 4(b), respectively. The ratio of the amplitudes (with a normalizing factor of 1.008) with 100% hydrogen and 100% air, and the difference in phases between the two, taken at different frequencies are shown as discrete points in Figs. 2(a) and 2(b), respectively. This shows that the frequency dependence of the signal is in good agreement with the theory, confirming the suggested mechanism. At high frequencies the poor signal-to-noise ratio of the pyroelectric signal led to larger errors in the measurement of the signal change due to hydrogen. The deviations from the theory at high frequencies are within the error bars of the measurement.

The experimentally obtained amplitude ratio and phase difference with respect to 100% air as a function of hydrogen percentage in air is shown as discrete squares in Figs. 5(a) and 5(b), respectively. These data seem to fit best a theoretical curve (solid line) calculated from Eqs. (14) and (15) assuming a relationship between the thermal coupling coefficient $b_{gf}=b_{H2}$ and the hydrogen concentration in air, $[H_2]$, given by

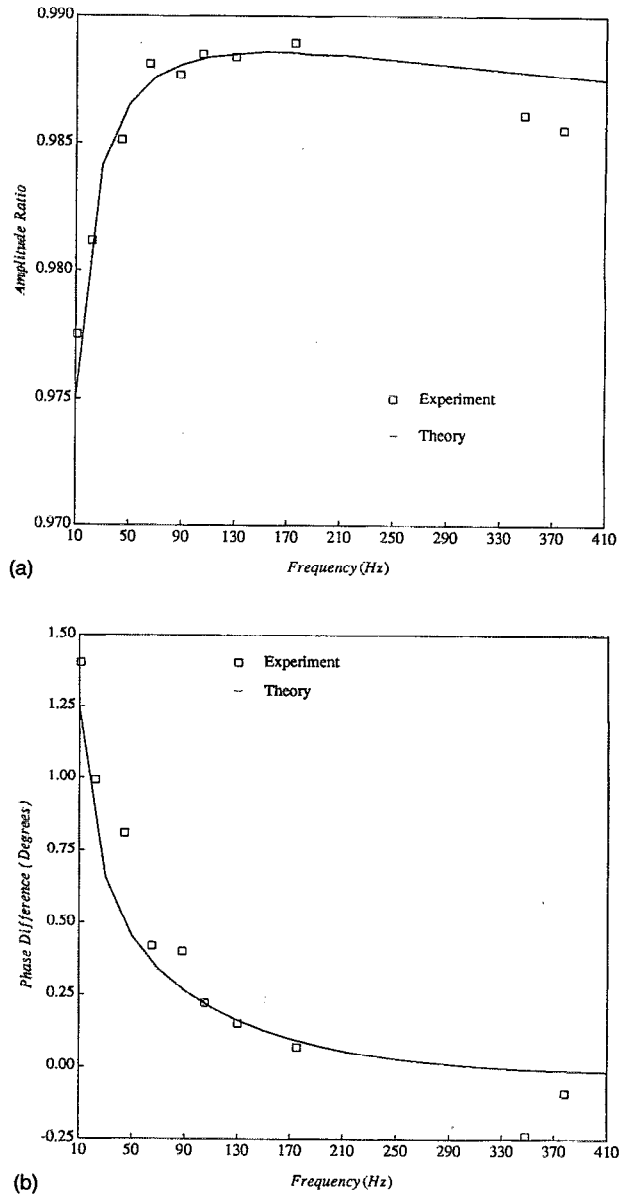

FIG. 2. Theoretical (solid line) and experimental (discrete squares) (a) amplitude ratio; and (b) phase difference, with 100% hydrogen and 100% air as a function of frequency. The experimental amplitude data have been normalized by a factor 1.008.

TABLE I. Phase difference and amplitude ratio with respect to pure air for various pure gases at STP. The percentage change in phase with reference to the phase change due to 100% hydrogen is given in parentheses.

Gas	Phase(Gas)−Phase(Air) (% w.r.t. H_2)	Amp.(Gas)/Amp.(Air)
Hydrogen (H_2)	$+8.210\times10^{-1}$(100%)	0.9818
Helium (He)	$+5.303\times10^{-1}$(64.5%)	0.9883
Ammonia (NH_3)	$+4.799\times10^{-3}$(0.58%)	0.9989
Oxygen (O_2)	$+7.463\times10^{-3}$(0.91%)	0.9998
Nitrogen (N_2)	-3.260×10^{-3}(−0.40%)	1.0001
Carbon monoxide (CO)	-1.185×10^{-2}(−1.44%)	1.0003
Carbon dioxide (CO_2)	-5.150×10^{-2}(−6.27%)	1.0011

$$b_{H2}=\sqrt{[H_2]}. \tag{17}$$

A comparison between Eqs. (11) and (17) strongly suggests that the photopyroelectric signal in the presence of a given concentration of hydrogen gas in air can be attributed to the change in the gas mixture thermal conductivity, which, in turn, affects the interfacial thermal coupling coefficient of the photothermal wave field. The variation of the gas conductivity seems to be linear with $[H_2]$ in the hydrogen concentration range of our experiment (12%–100% in air):

$$k_{H2}\propto[H_2]. \tag{18}$$

IV. DISCUSSION

In this paper we have demonstrated a new photopyroelectric gas sensor whose sensitivity is based on the thermal properties of the gas. This device is inexpensive and easy to construct using standard commercially available components. It has shown reliability, reversibility, and excellent stability against drift in the thermal wave phase detection mode. No hot igneous filament or other combustible elements are involved and, therefore, the new sensor is a good candidate for safe hydrogen detection in open ambients. The PVDF device is based on ac thermal wave propagation in the bulk of the pyroelectric element and the signal is measured at a fixed frequency, thus eliminating ambient transient thermal effects and dc drifts, such as those exhibited by the TDC. It is also immune to background temperature fluctuations or mechanical vibrations. The temperature elevation of the PVDF sensor film due to laser heating is extremely small (<1 K), a feature which gives the new sensor a definite advantage for safe hydrogen sensing. Table I suggests that

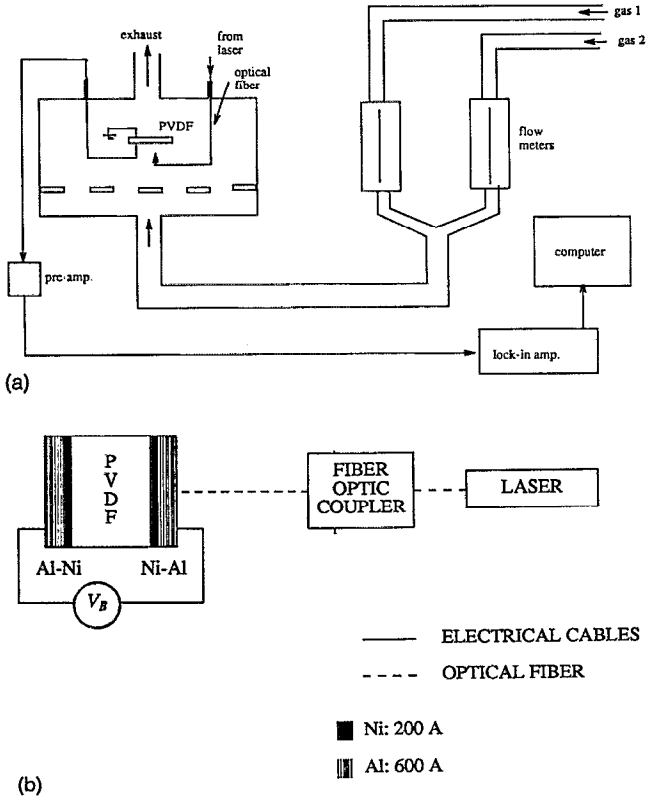

FIG. 3. (a) Schematic of the experimental setup. (b) Geometry of the active PVDF device.

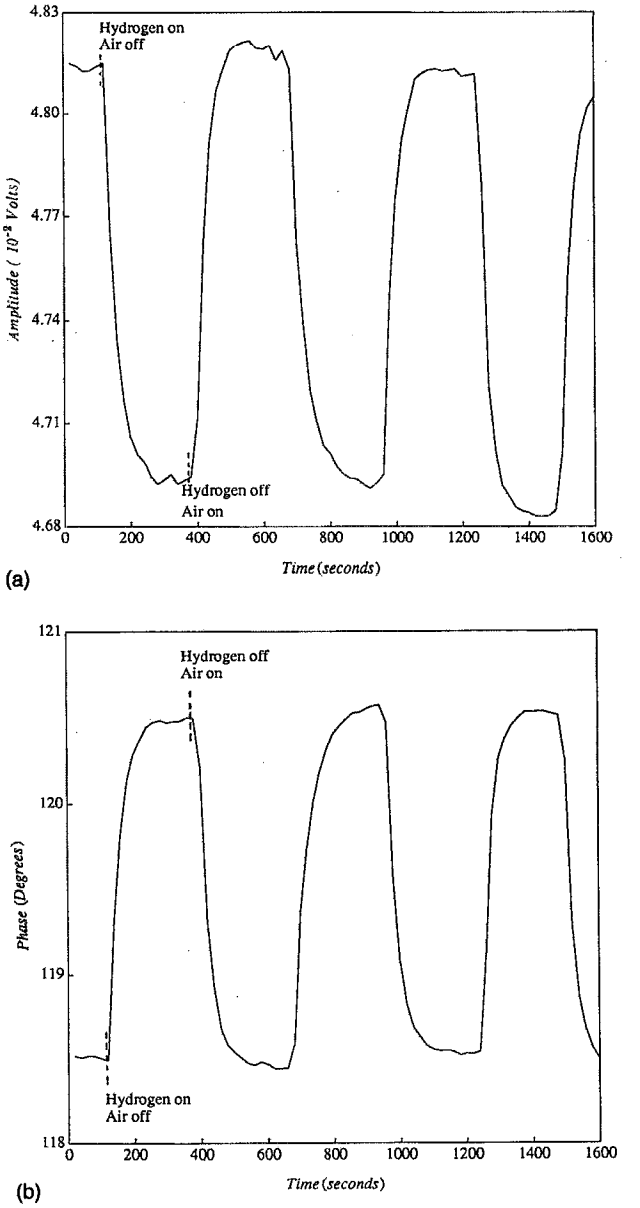

FIG. 4. (a) Amplitude and the (b) phase signal from the lock-in amplifier for several cycles of pure hydrogen and pure air.

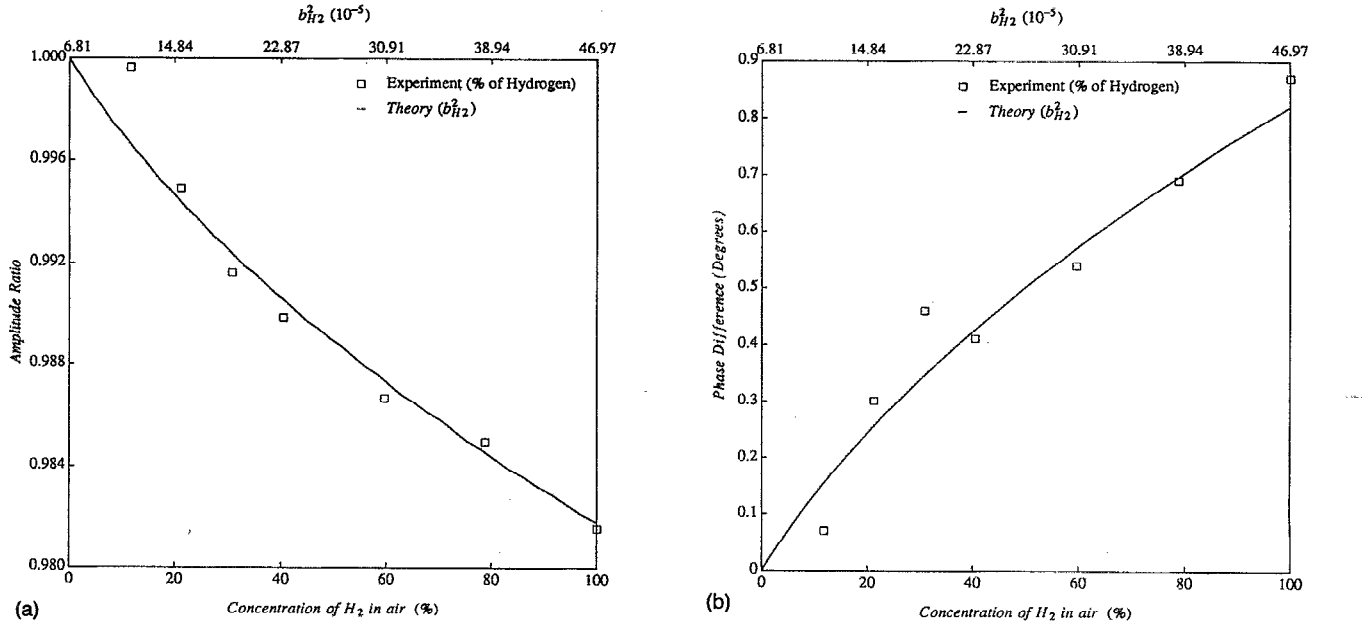

FIG. 5. Experimental (discrete points) (a) amplitude ratio and (b) phase difference with respect to pure air as a function of percentage of hydrogen in air and the corresponding theoretical (sold lines) signal as a function of b_{H2} (empirical guess). Here, experimental amplitude has been normalized by a factor 1.008 and the phase has been shifted by -0.22 deg.

this sensor shows good sensitivity to hydrogen in the presence of other common gases except helium, at STP. One problem common to photopyroelectric[13] and other[6] hydrogen sensors where Pd is used is the aging of the sensor. In H_2–O_2 mixtures catalytic behavior of Pd enhances the formation of water, blocking the Pd surface.[14] These problems are not expected in the new device. One disadvantage of this sensor, however, may be its lower selectivity than its Pd-coated counterpart.[7] This anticipated problem is expected to be overcome, at least partially, with calibration of the sensor under several ambient gases.

ACKNOWLEDGMENT

The support of the Ministry of Energy, Mines and Resources Canada through a contract to CHES is gratefully acknowledged.

[1] K. I. Lundstrom, M. S. Shivaraman, and C. M. Svensson, Surf. Sci. **64**, 497 (1977).
[2] M. C. Steele and B. A. MacIver, Appl. Phys. Lett. **28**, 687 (1976).
[3] A. D'Amico, G. Fortunato, and G. Petrocco, Sensors and Actuators **4**, 349 (1983).
[4] T. L. Poteat and B. Lalevic, IEEE Trans. Electron Devices **ED-29**, 123 (1982).
[5] A. Mandelis and C. Christofides, Sensors and Actuators **B2**, 79 (1990).
[6] C. Christofides and A. Mandelis, J. Appl. Phys. **68**, R1 (1990).
[7] A. Mandelis and C. Christofides, *Physics and Chemistry of Solid-State Gas Sensors, Chemical Analysis*, edited by J. D. Winefordner (Wiley, New York, in press).
[8] KYNAR Piezo Film Technical Manual, Pennwalt Corp., King of Prussia, PA (1983).
[9] A. Mandelis and C. Christofides, J. Appl. Phys. **70**, 4496 (1991).
[10] G. A. Shakespear, Proc. R. Phys. Soc. London **33**, 163 (1921).
[11] G. Guiochon and C. L. Guillemin, *Quantitative Gas Chromatography for Laboratory Analysis and On-Line Process Control* (Elsevier, New York, 1988); J. Chrom. Lib. **42**, p. 423.
[12] J. H. Lienhard, *A Heat Transfer Textbook* (Prentice-Hall, Englewood Cliffs, NJ, 1981), p. 500.
[13] C. Christofides, A. Mandelis, and J. Enright, Jpn. J. Appl. Phys. **30**, 2916 (1991).
[14] R. C. Hughes, W. K. Schubert, T. E. Zipperian, J. L. Rodriguez, and T. A. Plut, J. Appl. Phys. **62**, 1074 (1987).